Atmos. Chem. Phys., 19, 1–14, 2019
https://doi.org/10.5194/acp-19-1-2019

Atmospheric Chemistry and Physics
Open Access
EGU

The significant contribution of HONO to secondary pollutants during a severe winter pollution event in southern China

Xiao Fu[1], Tao Wang[1], Li Zhang[1,2], Qinyi Li[1,a], Zhe Wang[1], Men Xia[1], Hui Yun[1], Weihao Wang[1], Chuan Yu[1], Dingli Yue[3], Yan Zhou[3], Junyun Zheng[4], and Rui Han[5]

[1]Department of Civil and Environmental Engineering, Hong Kong Polytechnic University, Hong Kong 99907, China
[2]Atmospheric and Oceanic Sciences, Princeton University, Princeton, New Jersey 08540, USA
[3]Guangdong Provincial Environmental Monitoring Center, Guangzhou, China
[4]Institute for Environmental and Climate Research, Jinan University, Guangzhou, China
[5]National Meteorological Information Center, China Meteorological Administration, Beijing 100081, China
[a]now at: Department of Atmospheric Chemistry and Climate, Institute of Physical Chemistry Rocasolano, CSIC, Madrid 28006, Spain

Correspondence: Tao Wang (tao.wang@polyu.edu.hk)

Received: 16 August 2018 – Discussion started: 17 September 2018
Revised: 25 November 2018 – Accepted: 10 December 2018 – Published: 2 January 2019

Abstract. Nitrous acid (HONO) can strongly affect atmospheric photochemistry in polluted regions through the production of hydroxyl radicals (OHs). In January 2017, a severe pollution episode occurred in the Pearl River Delta (PRD) of China, with maximum hourly $PM_{2.5}$, ozone, and HONO levels reaching 400 µg m^{-3}, 150 ppb, and 8 ppb, respectively, at a suburban site. The present study investigated the sources and processes generating such high HONO concentrations and the role of HONO chemistry in this severe winter episode. Four recently reported HONO sources were added to the Community Multiscale Air Quality (CMAQ) model, including RH-dependent (relative humidity) and light-enhancing effects on heterogeneous reactions, photolysis of particulate nitrate in the atmosphere, and photolysis of HNO_3 and nitrate on surfaces. The revised model reproduced the observed HONO and significantly improved its performance for O_3 and $PM_{2.5}$. The model simulations showed that the heterogeneous generation on surfaces (with RH and light effects) was the largest contributor (72 %) to the predicted HONO concentrations, with the RH-enhancing effects more significant at nighttime and the light-enhancing effects more important in the daytime. The photolysis of total nitrate in the atmosphere and deposited on surfaces was the dominant HONO source during noon and afternoon, contributing above 50 % of the simulated HONO. The HONO photolysis was the dominant contributor to HO_x production in this episode. With all HONO sources, the daytime average O_3 at the Heshan site was increased by 24 ppb (or 70 %), compared to the simulation results without any HONO sources. Moreover, the simulated mean concentrations of TNO_3 (HNO_3+ fine particle NO_3^-) at the Heshan site, which was the key species for this haze formation, increased by about 17 µg m^{-3} (67 %) due to the HONO chemistry, and the peak enhancement reached 55 µg m^{-3}. This study highlights the key role of HONO chemistry in the formation of winter haze in a subtropical environment.

1 Introduction

Nitrous acid (HONO) can significantly affect atmospheric photochemistry through its photolysis producing hydroxyl radicals (OHs) (Reaction R1) and subsequent reactions of OH with other gases (Alicke et al., 2003; Kleffmann et al., 2005). OH radicals oxidize volatile organic compounds (VOCs) and convert nitric oxide (NO) into nitrogen dioxide (NO_2) without consuming ozone (O_3), leading to the generation of O_3 (Reactions R2 to R6). The oxidation of oxides of nitrogen ($NO_x = NO + NO_2$), sulfur dioxide (SO_2), and VOCs by OH and O_3 also produce secondary aerosols, which are the key components of haze (e.g., Pathak et al., 2009, 2011;

Cao et al., 2012).

$$\mathrm{HONO} + h\nu \rightarrow \mathrm{NO} + \mathrm{OH} \quad \text{(R1)}$$

$$\mathrm{OH} + \mathrm{VOC} \rightarrow \mathrm{RO_2} + \mathrm{H_2O} \quad \text{(R2)}$$

$$\mathrm{RO_2} + \mathrm{NO} \rightarrow \mathrm{NO_2} + \mathrm{HO_2} + \mathrm{OVOC} \quad \text{(R3)}$$

$$\mathrm{HO_2} + \mathrm{NO} \rightarrow \mathrm{NO_2} + \mathrm{OH} \quad \text{(R4)}$$

$$\mathrm{NO_2} + h\nu \rightarrow \mathrm{NO} + \mathrm{O^3P} \quad \text{(R5)}$$

$$\mathrm{O^3P} + \mathrm{O_2} \rightarrow \mathrm{O_3} \quad \text{(R6)}$$

The impact of HONO on atmospheric photochemistry varies under different environmental conditions. In general, the effect of HONO is more significant in polluted conditions than clean conditions. For example, calculations constrained by field measurements of HONO have suggested that the contributions of HONO photolysis to the daytime HO_x ($HO_x = OH + HO_2$) production can reach 56 % in an urban area (Ren et al., 2003) and 87 % at a roadside (Yun et al., 2017), which are higher than the contributions in rural and forested areas (30 % to 40 %) (Acker et al., 2006; Kleffmann et al., 2005). Simulations by chemistry transport models which considered major sources of HONO showed that the maximum enhancements of O_3 concentrations due to HONO were mostly less than 10 ppb in the US and other Western countries (Sarwar et al., 2008; Czader et al., 2012; Li et al., 2010; Goncalves et al., 2012), but more significant impacts have been reported in China due to more intense NO_x and VOC emissions. For example, the reported maximum hourly O_3 enhancement can be more than 30 ppb in Beijing (Li et al., 2011; Xu et al., 2006) and up to 25 ppb in Hong Kong (Zhang et al., 2016). The previous studies mostly focused on summertime. Limited attention has been paid to the winter season when the observed HONO concentrations can also be high (Hou et al., 2016; Li et al., 2018a; Wang et al., 2016; Xu et al., 2015).

The source and formation mechanisms of HONO are still not fully understood. Most previous studies suggest that a heterogeneous reaction of NO_2 on the surface is dominant, especially at night (Li et al., 2012; J. Wang et al., 2017; Zhang et al., 2016). In the daytime, the long-known gas-phase reaction of NO and OH explains less than 10 % of the daytime HONO production (Sarwar et al., 2008; Li et al., 2010; Zhang et al., 2016). Other daytime sources include direct traffic emissions (Kurtenbach et al., 2001; Liang et al., 2017), humidity- and light-dependent heterogeneous generation (Finlayson-Pitts et al., 2003; Ndour et al., 2008; Monge et al., 2010), soil emissions (Oswald et al., 2013; Su et al., 2011; Meusel et al., 2018), photolysis of particle nitrate in the atmosphere (Ye et al., 2016b, 2017), and photolysis of deposited HNO_3 and nitrate on the ground (Ye et al., 2016a; Zhou et al., 2011).

During 4–8 January 2017, a severe winter air pollution event occurred in the Pearl River Delta (PRD), a region long known to suffer from photochemical pollution due to its fast industrialization (Chan and Yao, 2008; Wang et al., 1998, 2003; T. Wang 2017; Xue et al., 2014; Zhang et al., 2008; Zheng et al., 2010). During this multiday episode, an hourly peak value of $\sim$ 150 ppb for O_3 and $\sim 400\,\mu g\,m^{-3}$ for $PM_{2.5}$ were observed, and the HONO levels reached 8 ppb, with an average value of 2.9 ppb at night (18:00 to 06:00 LT) and 2.4 ppb in daytime (07:00 to 17:00 LT). The HONO values were among the highest ever reported in China (Bernard et al., 2016; Huang et al., 2017; Li et al., 2012, 2018a; Qin et al., 2009; Su et al., 2008; J. Wang et al., 2017, 2013; Xu et al., 2015). It is of great interest to find out how such a high level of HONO was produced and what impact it had on the radical levels and secondary pollutants during this severe winter pollution event.

The present study utilizes the Community Multiscale Air Quality (CMAQ) model with up-to-date HONO sources, including those in the original CMAQ model (gas-phase generation, heterogeneous reaction, and vehicle emissions) and four newly added sources (RH-enhancing effects on heterogeneous reactions, light-enhancing effects on heterogeneous reactions, photolysis of particulate nitrate in the atmosphere, and photolysis of HNO_3 and nitrate adsorbed on surfaces). The updated model was then used to analyze the contributions of different HONO sources and also to quantify the contributions of HONO to secondary pollutants during this severe winter pollution event. Our study reveals the very large impact of HONO on winter-time chemistry at this subtropical site.

2 Materials and methods

2.1 Model description

2.1.1 CMAQ model configurations and inputs

CMAQ version 5.1 with the updated carbon bond 2005 e51 (CB05e51) gas mechanism and AERO6 aerosol mechanism (Appel et al., 2017) was used in this study. One-way triple nesting domains were used with their horizontal resolutions being 36, 12, and 4 km, respectively, and the innermost domain (domain 3) covers the PRD region (Fig. 1). These domains are based on a Lambert projection with two true latitudes of 25 and 40° N. The objective simulation period was 4 to 8 January 2017, with 6 days before as a spin-up time.

The Weather Research and Forecasting (WRF) Model version 3.7 was applied to generate the meteorological fields for the CMAQ simulations. The physical options used in the WRF model were the Lin microphysics scheme (Lin et al., 1983), the Rapid Radiative Transfer Model for GCMs (RRTMG) shortwave and longwave radiation scheme (Mlawer and Clough, 1998; Mlawer et al., 1997), Noah land surface scheme (Chen and Dudhia, 2001), YSU PBL scheme (Hong et al., 2006), and Kain–Fritsch cumulus scheme (Kain, 2004). To improve the meteorological modeling performance, the nudging was performed using the NCEP Au-

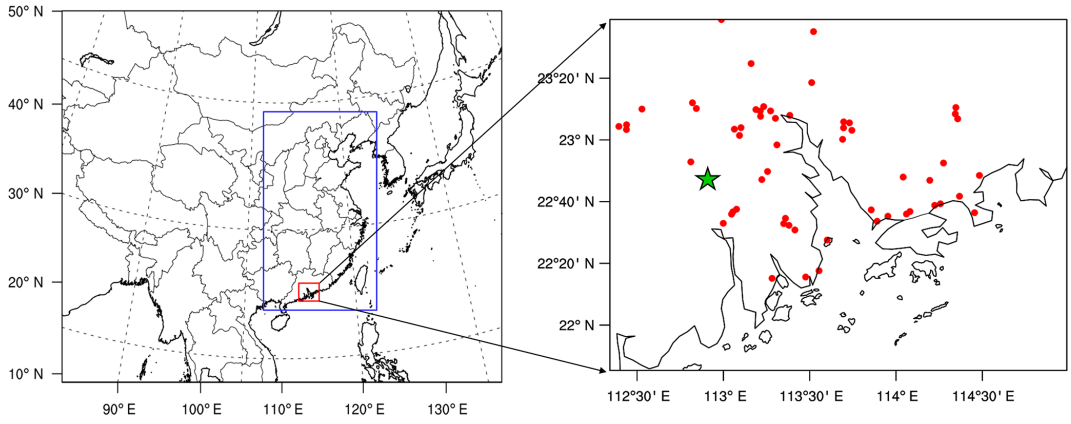

Figure 1. Model domains and locations of the monitoring sites. The green star represents the Heshan site and red dots represent official monitoring sites in the PRD region from the Ministry of Ecology and Environment of China.

tomated Data Processing (ADP) data (ds351.0 and ds461.0) and surface observation data from China Meteorological Administration (Zhang et al., 2016). Table S1 in the Supplement summarizes the statistical performance for the meteorological predictions.

The anthropogenic emission input was generated based on three emission inventories covering different regions. For the PRD region, a local emission inventory with high resolution for 2010 (Pan et al., 2014) was used. For other regions in China, the emission data for 2013 were from Ma et al. (2017). For other Asian countries, the INTEX-B dataset (Zhang et al., 2009) was used. HONO emissions from transportation sources were calculated based on the HONO / NO_x ratios and NO_x emissions from the transportation sources in the anthropogenic emission inventory. The HONO / NO_x ratios were set as 0.8 % and 2.3 % for gasoline and diesel engines, respectively (Kurtenbach et al., 2001; Gutzwiller et al., 2002). Natural biogenic emissions were estimated by the Model of Emissions of Gases and Aerosols from Nature (MEGAN) (Guenther et al., 2006).

2.1.2 Parameterization of HONO sources

In addition to the direct anthropogenic emissions, the default CMAQ model has two more HONO sources, including the gas-phase homogeneous reaction of NO and OH (Reaction R7) and the heterogeneous reactions of NO_2 on surfaces (Reaction R8) (Sarwar et al., 2008). The heterogeneous formation of HONO on the particle, urban, and leaf surfaces was estimated with a reaction rate $k = 5 \times 10^{-5} \times (S/V)$ as measured by Kurtenbach et al. (2001) under dark conditions with a relative humidity (RH) of 50 %.

$$NO + OH \rightarrow HONO \quad (R7)$$

$$2NO_2 + H_2O \xrightarrow{\text{surface}} HONO + HNO_3 \quad (R8)$$

In the present study, we incorporated four additional HONO sources, as described below.

1. *RH-enhancing effects on the heterogeneous reaction of NO_2 on surfaces*

   The default heterogeneous reaction rate was based on measurements at a relative humidity of 50 %. However, previous field and lab studies found that surface adsorbed water played a key role in the heterogeneous conversion and the reaction rate was highly dependent on the RH level (Finlayson-Pitts et al., 2003; Stutz et al., 2004; Qin et al., 2009). The laboratory measurements over an RH range of 0 % to 80 % conducted by Finlayson-Pitts et al. (2003) showed that the heterogeneous conversion rate increased much faster when RH $\geq$ 50 % than that when RH $<$ 50 %. Based on this result, the RH dependence of the heterogeneous reaction was considered through scaling the default reaction rate by a factor of f_{RH} in this study, as shown in the following equation:

$$k_{het} = 5 \times 10^{-5} \times f_{RH} \times (S/V) \quad (E1)$$

$$f_{RH} = \begin{cases} RH/50 & (RH < 50) \\ RH/10 - 4 & (50 \leq RH < 80) \\ 4 & (RH \geq 80)\,. \end{cases}$$

2. *Light-enhancing effects on the heterogeneous reaction of NO_2 on surfaces*

   The default reaction rate coefficient for the heterogeneous reaction was based on measurements under dark conditions. However, it has been reported that sunlight significantly boosts the heterogeneous generation of HONO (Ndour et al., 2008; Monge et al., 2010; Stemmler et al., 2007). To consider the photo-enhancing effect, we applied a higher reaction rate at daytime (Li et al., 2010; Czader et al., 2012), as shown in the following equation:

$$k_{het} = 1 \times 10^{-3} \times \frac{\text{light intensity}}{400} \times (S/V)\,, \quad (E2)$$

where light intensity means the total downward irradiance at the surface, measured in watts per meter squared ($W\,m^{-2}$).

3. *Photolysis of particulate nitrate in the atmosphere*

   Evidence from recent aircraft observations and laboratory measurements suggested that particulate nitrate in the atmosphere can undergo photolysis to produce HONO and NO_2 (Reaction R9) (Ye et al., 2016b, 2017).

$$pNO_3 \rightarrow 0.67\mathrm{HONO} + 0.33NO_2 \quad \text{(R9)}$$

   Ye et al. (2017) reported the photolysis rates ranging from 6.2×10^{-6} to $5.0 \times 10^{-4}\,s^{-1}$, with a median of $8.3 \times 10^{-5}\,s^{-1}$ at noontime tropical conditions. The reported value was much higher than the photolysis rate of gaseous HNO_3 ($\sim 7 \times 10^{-7}\,s^{-1}$) under the typical tropical noontime conditions (Finlayson-Pitts and Pitts, 2000; Ye et al., 2017). Similar to the methodology of Sarwar et al. (2008), the photolysis rate of particulate nitrate was estimated as the following equation:

$$J_{\mathrm{PNO3}} = \frac{8.3 \times 10^{-5}}{7 \times 10^{-7}} \times J_{\mathrm{HNO3-CMAQ}}, \quad \text{(E3)}$$

   where $J_{\mathrm{HNO3-CMAQ}}$ is the photolysis rate of gaseous HNO_3 calculated online in CMAQ.

4. *Photolysis of HNO_3 and nitrate deposited on surfaces*

   Field observations and lab studies also indicated that the photolysis of HNO_3 and nitrate deposited on the surface could be an important daytime HONO source (Reaction R10) (Zhou et al., 2003, 2011; Baergen and Donaldson, 2013). Ye et al. (2016a) tested the photolysis of HNO_3 and nitrate deposited on various natural and artificial surfaces in the laboratory, and reported the photolysis rates ranging from 6×10^{-6} to $3.7 \times 10^{-4}\,s^{-1}$, with a median of $3.4 \times 10^{-5}\,s^{-1}$.

$$\mathrm{deposited\_HNO_3/nitrate} \rightarrow 0.67\ \mathrm{HONO} + 0.33NO_2 \quad \text{(R10)}$$

   This reaction was incorporated into the CMAQ model by assuming deposited HNO_3 and nitrate on surfaces to equal the accumulation of dry deposition since the last precipitation event, referring to the method of Sarwar et al. (2008). The photolysis rate of deposited HNO_3 and nitrate was estimated as the following equation:

$$J_{\mathrm{DNO3}} = \frac{3.4 \times 10^{-5}}{7 \times 10^{-7}} \times J_{\mathrm{HNO3-CMAQ}}. \quad \text{(E4)}$$

2.1.3 Simulation cases

Eight simulations were conducted considering different HONO sources, including the following.

- NO_HONO: without any HONO sources
- G: gas-phase homogeneous reaction (G)
- GE: G + vehicle emissions (E)
- GEH (CMAQ default): GE + heterogeneous reactions under dark conditions with a RH of 50 % (H)
- GEHR: GEH + RH-enhancing effects on heterogeneous reactions (R)
- GEHRL: GEHR + light-enhancing effects on heterogeneous reactions (L)
- GEHRLP: GEHRL + photolysis of particulate nitrate in the atmosphere (P)
- GEHRLPD (CMAQ revised): GEHRLP + photolysis of HNO_3 and nitrate deposited on the surface (D)

2.2 Observation data

Field observations of HONO and other major air pollutants were conducted at the Heshan site (22°42′50″ N, 112°55′17″ E) in the PRD region (Fig. 1). Hourly HONO concentration was measured using a Long Path Absorption Photometer (LOPAP) (QUMA, Model LOPAP®-03) (Heland et al., 2001). The same instrument was employed by our group in several previous field campaigns (Zha et al., 2014; Xu et al., 2015; Liang et al., 2017; Yun et al., 2018). The reader referred to these sources (e.g., Yun et al., 2018) for description of measurement principle. Following our previous practice, the instrument background was determined with synthetic air four times a day, and calibrations with a nitrite solution standard were conducted every 3 days. The time resolution of this instrument was 10 min. The detection limit was 7 ppt with an accuracy of ±20 %. The sample inlets were placed at the roof of a four-floor building, at a height of about 15 m above the ground.

Other instruments whose data are used in the present paper have been summarized in Yun et al. (2018) with references provided for each instrument. Briefly, $PM_{2.5}$ concentrations were determined by a multiangle absorption photometer (Thermo Scientific, Model 5012). Sulfate, nitrate, and ammonium in $PM_{2.5}$ were measured by a gas and aerosol collector coupled with ion chromatography (GAC-IC) system. Gas HNO_3 concentrations were also measured by this GAC-IC system. O_3 concentrations were measured by a UV photometric analyzer (Thermo Scientific, Model 49i). NO_2 concentrations were measured using a chemiluminescence instrument (Thermo Scientific, Model 42i) coupled with a photolytic converter (Droplet Measurement Technologies, model BLC). The sample inlets for these instruments were placed at the same height as LOPAP.

Additionally, hourly $PM_{2.5}$, O_3, and NO_2 observation data at 56 official monitoring sites (Fig. 1) in the PRD region

Table 1. Model performance of the default and revised CMAQ model for O_3, $PM_{2.5}$, and NO_2 at 56 monitoring sites in the PRD region.

		OBS ($\mu g\,m^{-3}$)	SIM ($\mu g\,m^{-3}$)	Bias ($\mu g\,m^{-3}$)	NMB (%)	NME (%)	R
8h_max O_3	GEH (CMAQ default)	84.79	56.55	−28.24	−33.3	42.69	0.29
	GEHRLPD (CMAQ revised)		85.42	0.63	0.74	41.76	0.31
hourly $PM_{2.5}$	GEH (CMAQ default)	78.75	72.34	−6.40	−8.13	46.6	0.60
	GEHRLPD (CMAQ revised)		82.44	3.69	4.68	50.64	0.61
hourly NO_2[a]	GEH (CMAQ default)	53.39	64.39	11.00	20.61	49.51	0.64
	GEHRLPD (CMAQ revised)		58.42	5.03	9.42	43.75	0.67

[a] The NO_2 observation data were adjusted based on the method of Zhang et al. (2017): $NO_{2\,obs} = NO^{*}_{2\,obs} \times \frac{NO_{2\,sim}}{NO_{2\,sim}+NO_{z\,sim}-Nitrate_{sim}}$, where $NO^{*}_{2\,obs}$ is the measured concentration of NO_2 by the catalytic conversion technique; $NO_{2\,sim}$, $NO_{z\,sim}$, and $Nitrate_{sim}$ are the simulated concentrations of NO_2, NO_z, and nitrate.

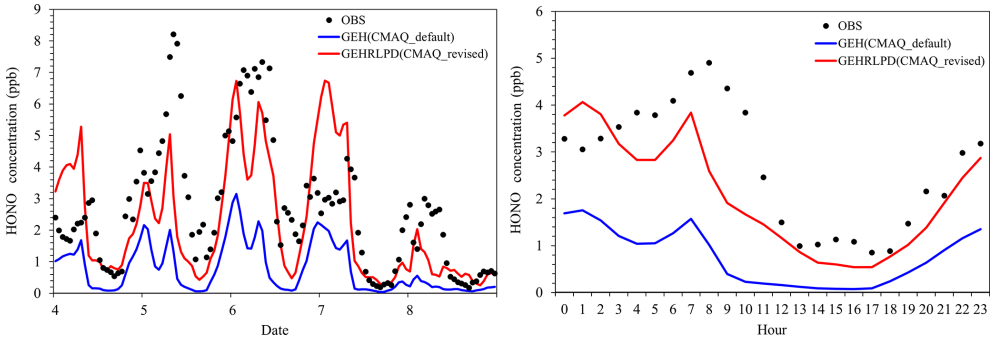

Figure 2. Observed and simulated HONO mixing ratios by the default and revised CMAQ model at the Heshan site during 4–8 January 2017.

were obtained from the Ministry of Ecology and Environment (MEE). It should be noted that NO_2 concentrations in the national network were measured using the catalytic conversion method, which overestimates NO_2, especially during the period with active photochemistry and at the location away from the primary emission sources (Xu et al., 2013). The NO_2 observation data were adjusted based on the method of Zhang et al. (2017) (also see footnote of Table 1).

3 Results and discussion

3.1 Observed pollution in this winter episode

During 4–8 January 2017, a severe pollution episode was observed in the PRD region. As shown in Fig. S1, the episode average $PM_{2.5}$ concentrations observed at the Heshan site reached $142\,\mu g\,m^{-3}$, which is nearly twice the respective standard of China ($75\,\mu g\,m^{-3}$ for daily average $PM_{2.5}$ concentration). The hourly $PM_{2.5}$ concentration peaked at $382\,\mu g\,m^{-3}$, which was among the highest $PM_{2.5}$ concentrations reported so far in the PRD region (Tan et al., 2009; Wang et al., 2012; Yue et al., 2015). O_3 levels were also high, with a peak of ~ 150 ppb. Figure S2 presented the spatial distribution of observed $PM_{2.5}$ and O_3 on the two heaviest polluted days (5 and 6 January) based on the interpolation of the observation data at the 56 official monitoring sites. It can be seen that the whole western PRD region suffered from severe pollution. On 5 January, the highest $PM_{2.5}$ pollution occurred in Foshan city and its surrounding area, with a peak of $448\,\mu g\,m^{-3}$. On 6 January, the pollution expanded to wider areas.

3.2 Evaluation of model performance

Figure 2 compared the simulated HONO mixing ratios by the default CMAQ model (GEH) and the revised CMAQ model (GEHRLPD) with the observations at the Heshan site for 4–8 January. For the HONO simulation, the default CMAQ significantly underestimated the levels, with a normalized mean bias (NMB) of −71.6 %. The maximum underestimation was 6 ppb in the early morning of 5 January. The simulated HONO levels in the afternoon were lower than 0.1 ppb in the default CMAQ model. By considering the four additional HONO sources, the model performance was improved considerably, with an NMB of −22.5 %. The simulated average daytime HONO mixing ratios increased from 0.37 to 1.44 ppb, and the simulated nighttime HONO values increased from 1.10 to 2.63 ppb. The revised model reproduced the HONO diurnal variation. Underestimation was found on the mornings of 5–6 and 8 January. One possible reason was

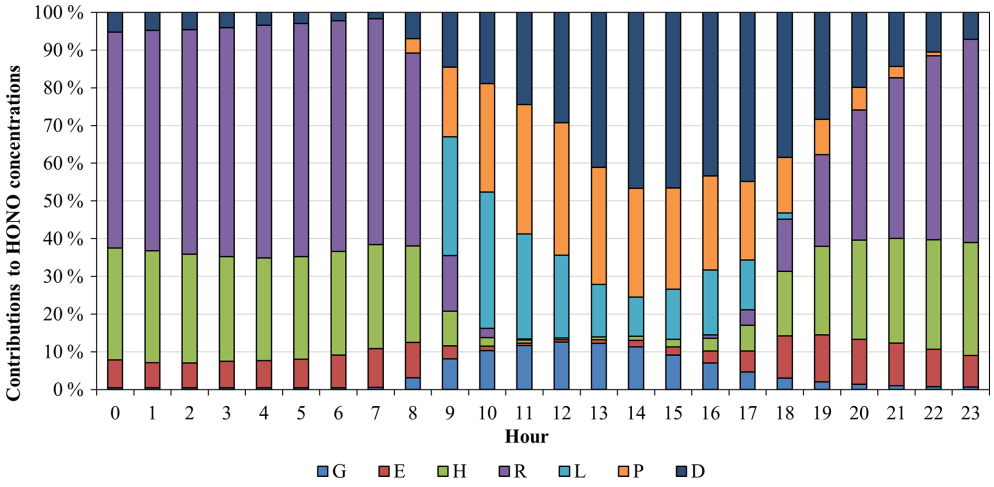

Figure 3. Average diurnal variations of contributions of different HONO sources to the simulated HONO mixing ratios at the Heshan site for 4–8 January 2017. The HONO sources include gas-phase homogeneous reaction of NO and OH (G), vehicle emissions (E), heterogeneous reactions under dark conditions with an RH of 50 % (H), RH-enhancing effects on heterogeneous reactions (R), light-enhancing effects on heterogeneous reactions (L), photolysis of particulate nitrate in the atmosphere (P), and photolysis of HNO_3 and nitrate deposited on the surface (D).

that some HONO sources were not considered in this study. For example, previous studies have proposed that deposited HONO can be reserved in dew water on the ground or vegetation during the night and re-released when the dew water evaporates in the morning (He et al., 2006). Here we have simply estimated HONO released from dew in the morning on 5 January during 00:00–08:00 LT using the method described in He et al. (2006). The total HONO dry deposition was 1.28×10^{-6} moles m^{-2}. At 09:00 LT, if 80 % of accumulated HONO was emitted to the surface model layer (about 0–30 m), the total released HONO amount would be 0.76 ppb. This suggests that dew evaporation may be a considerable source, but other sources may also exist. Overestimation was seen on the nights of 4 and 7 January, which was possibly related to some missing HONO sinks, e.g., the uptake of HONO on the ground surface (VandenBoer et al., 2014). Additionally, the overestimation of NO_2 could also partially explain the overestimation of HONO on the night of 7 January.

The inclusion of the four additional HONO sources also changed the model performance for other air pollutants. As shown in Fig. S1, the O_3 prediction by the default CMAQ model was not satisfactory, especially for the peak value. For example, on 6 January, the observed maximum 1 and 8 h O_3 mixing ratios at the Heshan site reached 147 and 125 ppb, respectively, exceeding the respective standard of China ($\sim$ 93 and 75 ppb for maximum 1 and 8 h O_3 concentrations, respectively). The simulated levels by the default CMAQ model were just 64 and 52 ppb, respectively, which failed to predict the noncompliance of O_3 for this episode. In contrast, the revised model was better to reproduce the magnitude. For the episode average, the NMB values decreased from -32.9 % to 5.5 % for the maximum 8 h O_3. Therefore, it is crucial to include these additional HONO sources into air quality models. For NO_2, the revised model could reproduce its temporal variation in general, although underestimation was seen for some peak NO_2 values. This underprediction could also partially explain the underestimation of HONO peak values. For $PM_{2.5}$, improvements also can be seen, especially for the peak values. For the sulfate, nitrate and ammonium components in $PM_{2.5}$, as shown in Fig. S3, the revised model performed well in reproducing their temporal variations, with correlation coefficients (R values) of 0.5, 0.7, and 0.7, respectively. Compared to the default CMAQ model, the NMB values decreased from -29.8 % to -10 %, -53.8 % to -41.2 %, and -32.9 % to -14.1 % for fine particle sulfate, nitrate and ammonium, respectively. Underestimation could be seen for particle nitrate, especially on 5 January. The possible reason was underestimation of the emissions of NH_3 or other alkaline species (e.g., Ca, K, Na), which led to gas HNO_3 not being converted to particle nitrate sufficiently. The model performance for total nitrate (TNO_3 = gaseous HNO_3 + fine particle nitrate) was satisfactory, with an NMB of -3.2 % and R of 0.8.

Regionally, as shown in Table 1, the simulation results of the revised CMAQ model were in better agreement with the observations, with the NMBs decreasing from -33.3 % to 0.7 %, -8.1 % to 4.7 %, and 20.6 % to 9.4 % for 8 h maximum O_3, hourly average $PM_{2.5}$, and hourly average NO_2 values, respectively.

We have conducted a sensitivity test to compare the simulations with those considering more recent emission by linearly adjusting the emissions based on the ratio of 2017 emissions to 2010 emissions for China reported in a very recent

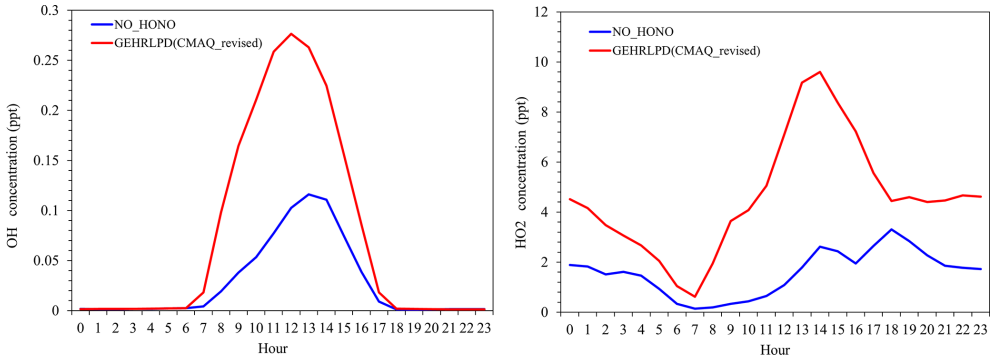

Figure 4. Average diurnal variations of OH and HO_2 mixing ratios simulated in the NO_HONO and GEHRLPD cases at the Heshan site during 4–8 January 2017.

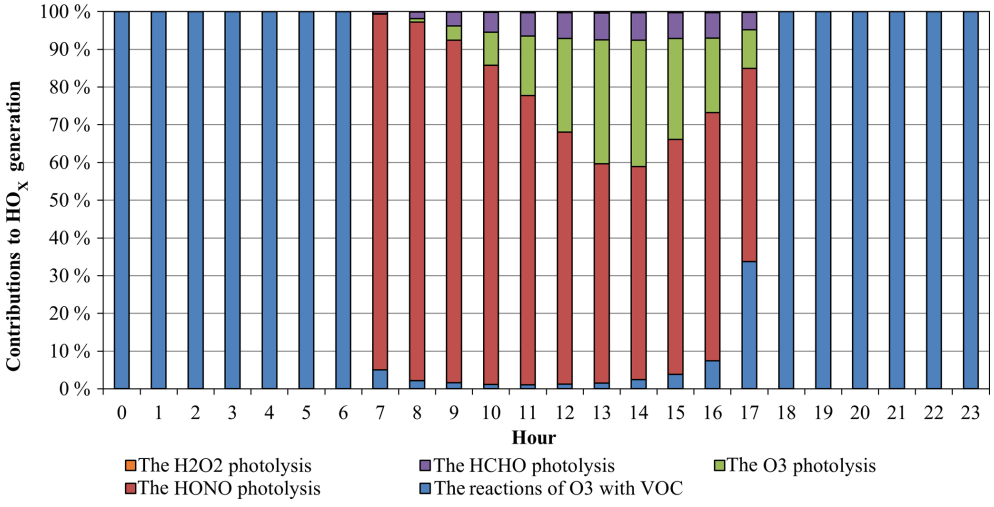

Figure 5. Average diurnal variations of contributions of different reactions to HO_x generation at the Heshan site.

paper (Zheng et al., 2018), but no improvements were indicated for HONO, O_3, and $PM_{2.5}$ at the Heshan site (Fig. S4). Despite the uncertainty, we think that the current emission setting is acceptable for simulations of the present case.

The above results indicated the satisfactory performance of the revised CMAQ model to simulate HONO and other major pollutants. It could be used to analyze the formation and impact of HONO in this episode.

3.3 Contributions of different sources to HONO concentrations

Figure 3 presents the contributions of different HONO sources to the HONO mixing ratios at the Heshan site. Heterogeneous generation on surfaces (including RH and light effects, H + R + L) was the largest contributor, representing 72 % of the average predicted HONO for the whole day. It contributed up to 81 % of the average predicted HONO values during the nighttime (18:00 to 06:00 LT) and ∼ 52 % during the daytime (07:00 to 17:00 LT). These findings on the dominant contribution from heterogeneous generation were

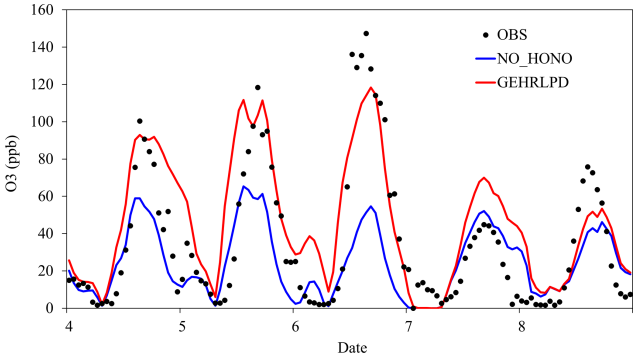

Figure 6. Temporal variation of observed and simulated O_3 mixing ratios in the NO_HONO and GEHRLPD cases at the Heshan site during 4–8 January 2017.

similar to those in the previous modeling studies (Sarwar et al., 2008; Zhang et al., 2016) and field measurements (Li et al., 2012; J. Wang et al., 2017). High relative humidity and solar radiation were two important driving factors for the for-

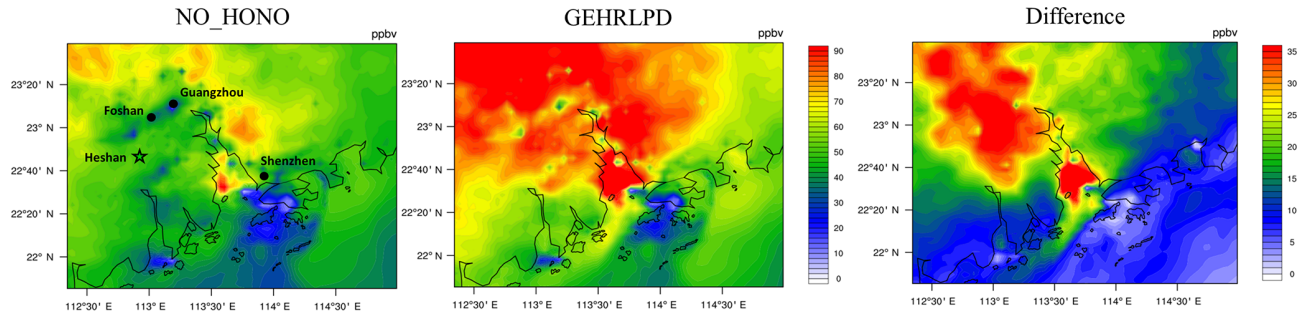

Figure 7. Spatial distributions of O_3 mixing ratios at 15:00 LT simulated in the NO_HONO and GEHRLPD cases and their difference for domain 3.

mation of the high HONO concentrations in this pollution episode. During the nighttime and early morning (18:00 to 08:00 LT), RH-enhancing effects on the heterogeneous generation were significant, due to high relative humidity (70 % to 90 %) (Fig. S5). The heterogeneous generation of HONO had a ∼ 2-fold increase by considering RH-enhancing effects, compared to that under the uniform relative humidity of 50 %. From 09:00 LT to the afternoon, light-enhancing effects became important, contributing approximately 25 % to HONO levels, due to strong radiation with a maximum of $\sim 450\,W\,m^{-2}$ (Fig. S5). In addition to enhancing the heterogeneous generation, the existence of light also increased HONO values through the photolysis of particle nitrate in the atmosphere and total nitrate deposited on the surface. Due to the high total nitrate concentrations in this pollution episode, these two photolysis sources were dominant during noon and afternoon (11:00 to 17:00 LT), contributing 31 % and 36 % to the HONO levels, respectively. Vehicle emissions contributed approximately 8 % of the daily average HONO values. The gas-phase homogeneous reaction was the smallest source, contributing approximately 3 % and 7 % of the daily and daytime average HONO values, respectively. Our model simulations suggest that the three additional light-dependent sources (L + P + D) could be an important part of missing daytime sources for the present case.

3.4 Impacts of HONO chemistry on HO_x and O_3

The HO_x ($OH + HO_2$) radical plays a key role in the atmospheric photochemical process. The photolysis of HONO can produce OH radicals, and a fast conversion exists between OH and HO_2 radicals. Therefore, the photolysis of HONO can affect the abundance of HO_x radicals. Figure 4 presents the average diurnal OH and HO_2 variations based on the simulations with and without the HONO sources (NO_HONO vs. GEHRLPD). The diurnal pattern and magnitude of the simulated OH and HO_2 mixing ratios in the GEHRLPD case were comparable to the previous observations in the PRD region and other areas (Lu et al., 2012; Mao et al., 2010). Compared to the results of the NO_HONO simulation, the daytime average OH and HO_2 values were increased by 175 % and 336 %, respectively. The integrated reaction rate (IRR) analysis tool available in CMAQ was utilized to explore the contribution of HONO photolysis to HO_x radical production relative to other HO_x radical sources in the surface layer (∼ 0 to 30 m), including the reaction of H_2O with O (^1D) which comes from the photolysis of O_3, HCHO photolysis, H_2O_2 photolysis, and the reaction of O_3 with alkenes and biogenic VOCs. As shown in Fig. 5, HONO photolysis was the dominant HO_x source during the daytime at the Heshan site. The daytime average contribution of HONO photolysis to HO_x production was approximately 74 %, and the contribution during the morning could be above 90 %. With the increasing of O_3 concentrations from sunrise to afternoon, the contribution of the O_3 photolysis began to increase and reached a peak of 33.4 % at 14:00 LT. Compared to the reported results for summer in the previous studies (Czader et al., 2012; Mao et al., 2010; Tham et al., 2016; Xue et al., 2016; Li et al., 2018c), the contribution of HONO photolysis to HO_x was much larger in the present study, mainly due to the high HONO concentrations in this winter episode. For example, Xue et al. (2016) and Li et al. (2018c) reported daytime average contributions of less than 30 % from HONO photolysis at two sites in Hong Kong. Tham et al. (2016) showed a contribution of less than 50 % in the morning at a site in the North China Plain. In these cases, the HONO levels were relatively low, with the peak HONO levels ranging among 1–3 ppb. The high HONO concentrations at Heshan increased the contribution of HONO photolysis to the formation of HO_x in this winter pollution episode. A similar high contribution can be found in other winter studies with high HONO concentrations, e.g., Elshorbany et al. (2010).

The enhanced HO_x formation due to HONO chemistry could increase O_3 concentrations. As shown in Fig. 6, the simulated daytime average O_3 mixing ratio at the Heshan site in the GEHRLPD case was approximately 24 ppb (70 %) higher than that in the NO_HONO case, with a peak increase up to 60 ppb. The O_3 enhancement was much higher than the previous simulation results for the summer cases (Sarwar et al., 2008; Li et al., 2010; Zhang et al., 2016). In addition to higher HONO concentrations, another possible reason was

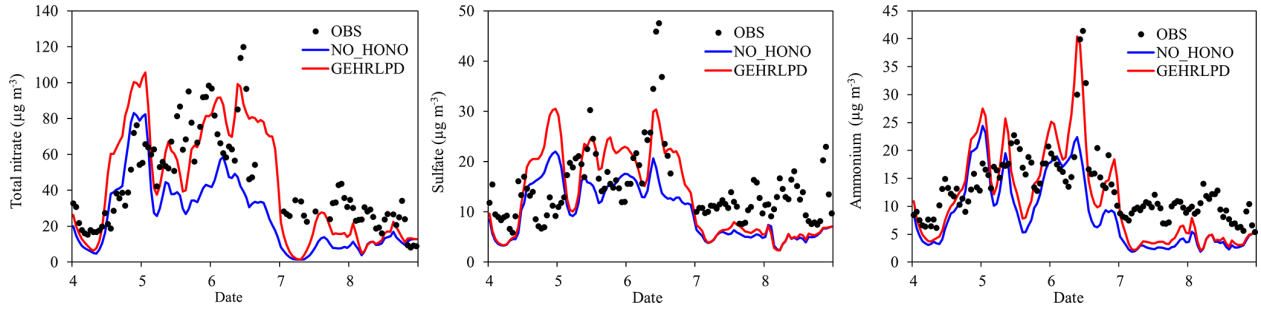

Figure 8. Temporal variation of observed and simulated total nitrate, sulfate, and ammonium concentrations in the NO_HONO and GEHRLPD cases at the Heshan site during 4–8 January 2017.

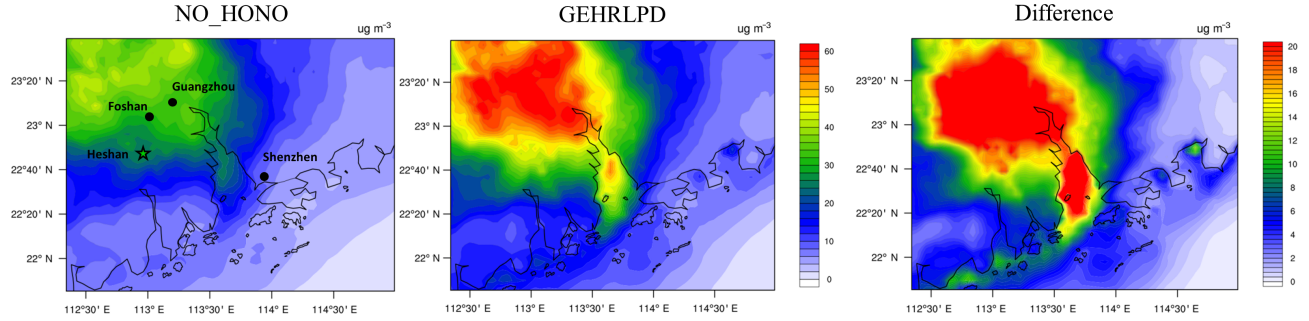

Figure 9. Spatial distributions of average TNO_3 concentrations simulated in the NO_HONO and GEHRLPD cases and their difference for domain 3 during 4–8 January 2017.

that the VOC / NO_x ratio was lower in winter than that in summer, due to less biogenic VOC emissions and more NO_x emission from fuel combustion in winter. For example, Zou et al. (2015) reported VOC / NO_x values higher than 10 : 1 in summer and about 5 : 1 for winter based on 1-year observation in Guangzhou, which is about 60 km from the Heshan site. The lower VOC / NO_x ratio increased the sensitivity of O_3 concentrations to HO_x changes through Reactions (2) to (4). Therefore, the enhancement of O_3 concentrations was more significant (Li et al., 2018b). Figure 7 presents the spatial distribution of simulated surface O_3 concentrations at 15:00 LT in the NO_HONO and GEHRLPD cases. With HONO sources, the increase of the regional average O_3 mixing ratio at 15:00 LT was 34 % (∼ 17 ppb). The above results indicated the significant impacts of HONO chemistry on the atmospheric oxidation capacity and O_3 pollution in the PRD region during this heavy winter episode.

3.5 Impacts of HONO chemistry on secondary inorganic aerosol formation

Secondary inorganic aerosols, including nitrate, sulfate, and ammonium, contributed approximately 50 % to $PM_{2.5}$ concentrations during this episode (Fig. S6). Among them, nitrate was the dominant component, with peak concentrations reaching ∼ 110 μg m^{-3}, which was much higher than the sulfate and ammonium concentrations. Particle nitrate can be generated through the partition of HNO_3 to particle phase. The major formation pathway of HNO_3 is the oxidation of NO_2 by OH during the daytime (Reaction R11). HNO_3 can also be produced via heterogeneous reactions of N_2O_5 on the particle surface at night (Reactions R12 to R14). Therefore, HONO chemistry can accelerate the formation of nitrate through the enhancement of atmospheric oxidation capacity (HO_x and O_3).

$$OH + NO_2 \rightarrow HNO_3 \quad \text{(R11)}$$

$$O_3 + NO_2 \rightarrow NO_3 \quad \text{(R12)}$$

$$NO_3 + NO_2 \rightarrow N_2O_5 \quad \text{(R13)}$$

$$N_2O_5 + H_2O \rightarrow 2HNO_3 \quad \text{(R14)}$$

Considering the uncertainty of the partition of gaseous HNO_3 to particle nitrate (see Sect. 3.2), we assessed the impact of HONO chemistry on the sum of HNO_3 and fine particle NO_3^- (TNO_3). As shown in Fig. 8, the average TNO_3 concentrations at the Heshan site increased by about 17 μg m^{-3} (67 %), and the peak enhancement reached 55 μg m^{-3} at 10:00 LT on 6 January, when the observed $PM_{2.5}$ and nitrate concentration was at its respective highest level. Figure 9 presents the distribution of simulated average surface TNO_3 concentrations in the NO_HONO and GEHRLPD case. With HONO sources, the regional average TNO_3 concentrations were increased by 8.4 μg m^{-3} for the entire episode. The absolute enhancement was more significant in the areas with higher

aerosol concentrations. The highest increase for TNO_3 was above $25\,\mu g\,m^{-3}$ for the episode average. Meanwhile, the HONO chemistry also accelerated the formation of other secondary inorganic aerosols. Particle sulfate can be generated through the partition of H_2SO_4 to the particle phase. The major formation pathways of H_2SO_4 include the gaseous oxidation of SO_2 by OH and the aqueous oxidation of S(IV) by O_3, H_2O_2, and other oxidants. The partition of gaseous NH_3 to particle ammonium was based on the $H_2SO_4-HNO_3-NH_3$ thermodynamic equilibrium. The simulated enhancements of the average sulfate and ammonium concentrations at the Heshan site were 32 % and 33 %, respectively. The above results indicated that the HONO chemistry also aggravated the particulate pollution during this episode.

4 Conclusions

This study has identified the major contributors to the observed high HONO levels during a severe winter pollution episode and highlighted the importance of HONO chemistry in the combined photochemical and haze pollution in a subtropical region. Including up-to-date HONO sources in the widely used CMAQ model significantly improved its capability in simulating ambient concentrations of HONO and other major pollutants (e.g., O_3 and $PM_{2.5}$). The model simulations suggested a predominant contribution from NO_2 heterogeneous reactions enhanced by humidity and solar radiation. The high HONO concentration significantly increased the atmospheric oxidation capacity and the levels of ozone and secondary aerosols, especially total nitrate. This study highlights the key role of HONO chemistry in the formation of winter haze in a subtropical environment and indicates the critical need to include and update HONO sources in regional air quality models in order to predict ozone and other secondary pollutants during heavy pollution events in southern China and similar regions. Additional efforts are needed to improve the current representation of HONO sources, such as evaporation of dew and a more accurate simulation of deposited nitrate.

Data availability. Model codes and input data are available from Xiao Fu. The measurement data used in this study are available from Tao Wang (cetwang@polyu.edu.hk) and Dingli Yue (dingliyue@163.com).

Supplement. The supplement related to this article is available online at: https://doi.org/10.5194/acp-19-1-2019-supplement.

Author contributions. TW and XF designed the research; XF performed model simulations and analysis; LZ and QL assisted in model simulations; YZ, DY, ZW, HY, MX, CY, and WW conducted measurements of trace gases and aerosol; JZ processed the PRD emission data; RH processed the weather data; XF and TW wrote the manuscript. All authors contributed to discussion and commented on the paper.

Competing interests. The authors declare that they have no conflict of interest.

Special issue statement. This article is part of the special issue "Regional transport and transformation of air pollution in eastern China". It is not associated with a conference.

Acknowledgements. We thank Miss Naiwen Zhang for her help in HONO measurement and the Environmental Protection Department of Hong Kong for loaning the LOPAP instrument. This work was sponsored by the Hong Kong Research Grants Council (C5022-14G and A-PolyU502/16).

Edited by: Dwayne Heard
Reviewed by: two anonymous referees

References

Acker, K., Moller, D., Wieprecht, W., Meixner, F. X., Bohn, B., Gilge, S., Plass-Dulmer, C., and Berresheim, H.: Strong daytime production of OH from HNO2 at a rural mountain site, Geophys. Res. Lett., 33, L02809, https://doi.org/10.1029/2005gl024643, 2006.

Alicke, B., Geyer, A., Hofzumahaus, A., Holland, F., Konrad, S., Patz, H. W., Schafer, J., Stutz, J., Volz-Thomas, A., and Platt, U.: OH formation by HONO photolysis during the BERLIOZ experiment, J. Geophys. Res.-Atmos., 108, 8247, https://doi.org/10.1029/2001jd000579, 2003.

Appel, K. W., Napelenok, S. L., Foley, K. M., Pye, H. O. T., Hogrefe, C., Luecken, D. J., Bash, J. O., Roselle, S. J., Pleim, J. E., Foroutan, H., Hutzell, W. T., Pouliot, G. A., Sarwar, G., Fahey, K. M., Gantt, B., Gilliam, R. C., Heath, N. K., Kang, D., Mathur, R., Schwede, D. B., Spero, T. L., Wong, D. C., and Young, J. O.: Description and evaluation of the Community Multiscale Air Quality (CMAQ) modeling system version 5.1, Geosci. Model Dev., 10, 1703–1732, https://doi.org/10.5194/gmd-10-1703-2017, 2017.

Baergen, A. M. and Donaldson, D. J.: Photochemical Renoxification of Nitric Acid on Real Urban Grime, Environ. Sci. Technol., 47, 815–820, https://doi.org/10.1021/es3037862, 2013.

Bernard, F., Cazaunau, M., Grosselin, B., Zhou, B., Zheng, J., Liang, P., Zhang, Y. J., Ye, X. N., Daele, V., Mu, Y. J., Zhang, R. Y., Chen, J. M., and Mellouki, A.: Measurements of nitrous acid (HONO) in urban area of Shanghai, China, Environ. Sci. Pollut. Res., 23, 5818–5829, https://doi.org/10.1007/s11356-015-5797-4, 2016.

Cao, J.-J., Shen, Z.-X., Chow, J. C., Watson, J. G., Lee, S.-C., Tie, X.-X., Ho, K.-F., Wang, G.-H., and Han, Y.-M.: Winter and Summer PM2.5 Chemical Compositions in Fourteen Chinese Cities, J. Air Waste Manage. Assoc., 62, 1214–1226, https://doi.org/10.1080/10962247.2012.701193, 2012.

Chan, C. K. and Yao, X.: Air pollution in mega cities in China, Atmos. Environ., 42, 1–42, https://doi.org/10.1016/j.atmosenv.2007.09.003, 2008.

Chen, F. and Dudhia, J.: Coupling an advanced land surface-hydrology model with the Penn State-NCAR MM5 modeling system. Part I: Model implementation and sensitivity, Mon. Weather Rev., 129, 569–585, https://doi.org/10.1175/1520-0493(2001)129<0569:caalsh>2.0.co;2, 2001.

Czader, B. H., Rappenglück, B., Percell, P., Byun, D. W., Ngan, F., and Kim, S.: Modeling nitrous acid and its impact on ozone and hydroxyl radical during the Texas Air Quality Study 2006, Atmos. Chem. Phys., 12, 6939–6951, https://doi.org/10.5194/acp-12-6939-2012, 2012.

Elshorbany, Y. F., Kleffmann, J., Kurtenbach, R., Lissi, E., Rubio, M., Villena, G., Gramsch, E., Rickard, A. R., Pilling, M. J., and Wiesen, P.: Seasonal dependence of the oxidation capacity of the city of Santiago de Chile, Atmos. Environ., 44, 5383–5394, https://doi.org/10.1016/j.atmosenv.2009.08.036, 2010.

Finlayson-Pitts, B. J. and Pitts Jr., J. N.: Chemistry of the Upper and Lower Atmosphere: Theory, Experiments, and Applications, Academic Press, San Diego, CA, 2000.

Finlayson-Pitts, B. J., Wingen, L. M., Sumner, A. L., Syomin, D., and Ramazan, K. A.: The heterogeneous hydrolysis of NO_2 in laboratory systems and in outdoor and indoor atmospheres: An integrated mechanism, Phys. Chem. Chem. Phys., 5, 223–242, https://doi.org/10.1039/b208564j, 2003.

Goncalves, M., Dabdub, D., Chang, W. L., Jorba, O., and Baldasano, J. M.: Impact of HONO sources on the performance of mesoscale air quality models, Atmos. Environ., 54, 168–176, https://doi.org/10.1016/j.atmosenv.2012.02.079, 2012.

Guenther, A., Karl, T., Harley, P., Wiedinmyer, C., Palmer, P. I., and Geron, C.: Estimates of global terrestrial isoprene emissions using MEGAN (Model of Emissions of Gases and Aerosols from Nature), Atmos. Chem. Phys., 6, 3181–3210, https://doi.org/10.5194/acp-6-3181-2006, 2006.

Gutzwiller, L., Arens, F., Baltensperger, U., Gaggeler, H. W., and Ammann, M.: Significance of semivolatile diesel exhaust organics for secondary HONO formation, Environ. Sci. Technol., 36, 677–682, https://doi.org/10.1021/es015673b, 2002.

He, Y., Zhou, X. L., Hou, J., Gao, H. L., and Bertman, S. B.: Importance of dew in controlling the air-surface exchange of HONO in rural forested environments, Geophys. Res. Lett., 33, L02813, https://doi.org/10.1029/2005gl024348, 2006.

Heland, J., Kleffmann, J., Kurtenbach, R., and Wiesen, P.: A new instrument to measure gaseous nitrous acid (HONO) in the atmosphere, Environ. Sci. Technol., 35, 3207–3212, https://doi.org/10.1021/es000303t, 2001.

Hong, S. Y., Noh, Y., and Dudhia, J.: A new vertical diffusion package with an explicit treatment of entrainment processes, Mon. Weather Rev., 134, 2318–2341, https://doi.org/10.1175/mwr3199.1, 2006.

Hou, S., Tong, S., Ge, M., and An, J.: Comparison of atmospheric nitrous acid during severe haze and clean periods in Beijing, China, Atmos. Environ., 124, 199–206, https://doi.org/10.1016/j.atmosenv.2015.06.023, 2016.

Huang, R. J., Yang, L., Cao, J. J., Wang, Q. Y., Tie, X. X., Ho, K. F., Shen, Z. X., Zhang, R. J., Li, G. H., Zhu, C. S., Zhang, N. N., Dai, W. T., Zhou, J. M., Liu, S. X., Chen, Y., Chen, J., and O'Dowd, C. D.: Concentration and sources of atmospheric nitrous acid (HONO) at an urban site in Western China, Sci. Total Environ., 593, 165–172, https://doi.org/10.1016/j.scitotenv.2017.02.166, 2017.

Kain, J. S.: The Kain-Fritsch convective parameterization: An update, J. Appl. Meteorol., 43, 170–181, https://doi.org/10.1175/1520-0450(2004)043<0170:tkcpau>2.0.co;2, 2004.

Kleffmann, J., Gavriloaiei, T., Hofzumahaus, A., Holland, F., Koppmann, R., Rupp, L., Schlosser, E., Siese, M., and Wahner, A.: Daytime formation of nitrous acid: A major source of OH radicals in a forest, Geophys. Res. Lett., 32, L05818, https://doi.org/10.1029/2005gl022524, 2005.

Kurtenbach, R., Becker, K. H., Gomes, J. A. G., Kleffmann, J., Lorzer, J. C., Spittler, M., Wiesen, P., Ackermann, R., Geyer, A., and Platt, U.: Investigations of emissions and heterogeneous formation of HONO in a road traffic tunnel, Atmos. Environ., 35, 3385–3394, https://doi.org/10.1016/s1352-2310(01)00138-8, 2001.

Li, D., Xue, L., Wen, L., Wang, X., Chen, T., Mellouki, A., Chen, J., and Wang, W.: Characteristics and sources of nitrous acid in an urban atmosphere of northern China: Results from 1-yr continuous observations, Atmos. Environ., 182, 296–306, https://doi.org/10.1016/j.atmosenv.2018.03.033, 2018a.

Li, G., Lei, W., Zavala, M., Volkamer, R., Dusanter, S., Stevens, P., and Molina, L. T.: Impacts of HONO sources on the photochemistry in Mexico City during the MCMA-2006/MILAGO Campaign, Atmos. Chem. Phys., 10, 6551–6567, https://doi.org/10.5194/acp-10-6551-2010, 2010.

Li, Q., Zhang, L., Wang, T., Wang, Z., Fu, X., and Zhang, Q.: "New" Reactive Nitrogen Chemistry Reshapes the Relationship of Ozone to Its Precursors, Environ. Sci. Technol., 52, 2810–2818, https://doi.org/10.1021/acs.est.7b05771, 2018b.

Li, X., Brauers, T., Häseler, R., Bohn, B., Fuchs, H., Hofzumahaus, A., Holland, F., Lou, S., Lu, K. D., Rohrer, F., Hu, M., Zeng, L. M., Zhang, Y. H., Garland, R. M., Su, H., Nowak, A., Wiedensohler, A., Takegawa, N., Shao, M., and Wahner, A.: Exploring the atmospheric chemistry of nitrous acid (HONO) at a rural site in Southern China, Atmos. Chem. Phys., 12, 1497–1513, https://doi.org/10.5194/acp-12-1497-2012, 2012.

Li, Y., An, J., Min, M., Zhang, W., Wang, F., and Xie, P.: Impacts of HONO sources on the air quality in Beijing, Tianjin and Hebei Province of China, Atmos. Environ., 45, 4735–4744, https://doi.org/10.1016/j.atmosenv.2011.04.086, 2011.

Li, Z., Xue, L., Yang, X., Zha, Q., Tham, Y. J., Yan, C., Louie, P. K. K., Luk, C. W. Y., Wang, T., and Wang, W.: Oxidizing capacity of the rural atmosphere in Hong Kong, Southern China, Sci. Total Environ., 612, 1114–1122, https://doi.org/10.1016/j.scitotenv.2017.08.310, 2018c.

Liang, Y. T., Zha, Q. Z., Wang, W. H., Cui, L., Lui, K. H., Ho, K. F., Wang, Z., Lee, S. C., and Wang, T.: Revisiting nitrous acid (HONO) emission from on-road vehicles: A tunnel study with a mixed fleet, J. Air Waste Manage. Assoc., 67, 797–805, https://doi.org/10.1080/10962247.2017.1293573, 2017.

Lin, Y. L., Farley, R. D., and Orville, H. D.: Bulk parameterization of the snow field in a cloud model, J. Clim. Appl. Meteorol., 22, 1065–1092, https://doi.org/10.1175/1520-0450(1983)022<1065:bpotsf>2.0.co;2, 1983.

Lu, K. D., Rohrer, F., Holland, F., Fuchs, H., Bohn, B., Brauers, T., Chang, C. C., Häseler, R., Hu, M., Kita, K., Kondo, Y., Li, X.,

Lou, S. R., Nehr, S., Shao, M., Zeng, L. M., Wahner, A., Zhang, Y. H., and Hofzumahaus, A.: Observation and modelling of OH and HO_2 concentrations in the Pearl River Delta 2006: a missing OH source in a VOC rich atmosphere, Atmos. Chem. Phys., 12, 1541–1569, https://doi.org/10.5194/acp-12-1541-2012, 2012.

Ma, Q., Cai, S., Wang, S., Zhao, B., Martin, R. V., Brauer, M., Cohen, A., Jiang, J., Zhou, W., Hao, J., Frostad, J., Forouzanfar, M. H., and Burnett, R. T.: Impacts of coal burning on ambient $PM_{2.5}$ pollution in China, Atmos. Chem. Phys., 17, 4477–4491, https://doi.org/10.5194/acp-17-4477-2017, 2017.

Mao, J. Q., Ren, X. R., Chen, S. A., Brune, W. H., Chen, Z., Martinez, M., Harder, H., Lefer, B., Rappengluck, B., Flynn, J., and Leuchner, M.: Atmospheric oxidation capacity in the summer of Houston 2006: Comparison with summer measurements in other metropolitan studies, Atmos. Environ., 44, 4107–4115, https://doi.org/10.1016/j.atmosenv.2009.01.013, 2010.

Meusel, H., Tamm, A., Kuhn, U., Wu, D., Leifke, A. L., Fiedler, S., Ruckteschler, N., Yordanova, P., Lang-Yona, N., Pöhlker, M., Lelieveld, J., Hoffmann, T., Pöschl, U., Su, H., Weber, B., and Cheng, Y.: Emission of nitrous acid from soil and biological soil crusts represents an important source of HONO in the remote atmosphere in Cyprus, Atmos. Chem. Phys., 18, 799–813, https://doi.org/10.5194/acp-18-799-2018, 2018.

Mlawer, E. J. and Clough, S. A.: Shortwave clear-sky model measurement intercomparison using RRTM, Proceedings of the 8 th Atmospheric Radiation Measurement (ARM) Science Team Meeting, Tucson, Arizona, USA, 1998.

Mlawer, E. J., Taubman, S. J., Brown, P. D., Iacono, M. J., and Clough, S. A.: Radiative transfer for inhomogeneous atmospheres: RRTM, a validated correlated-k model for the longwave, J. Geophys. Res.-Atmos., 102, 16663–16682, https://doi.org/10.1029/97jd00237, 1997.

Monge, M. E., D'Anna, B., Mazri, L., Giroir-Fendler, A., Ammann, M., Donaldson, D. J., and George, C.: Light changes the atmospheric reactivity of soot, Proc. Natl. Acad. Sci. USA, 107, 6605–6609, https://doi.org/10.1073/pnas.0908341107, 2010.

Ndour, M., D'Anna, B., George, C., Ka, O., Balkanski, Y., Kleffmann, J., Stemmler, K., and Ammann, M.: Photoenhanced uptake of NO_2 on mineral dust: Laboratory experiments and model simulations, Geophys. Res. Lett., 35, L05812, https://doi.org/10.1029/2007gl032006, 2008.

Oswald, R., Behrendt, T., Ermel, M., Wu, D., Su, H., Cheng, Y., Breuninger, C., Moravek, A., Mougin, E., Delon, C., Loubet, B., Pommerening-Roser, A., Sorgel, M., Poschl, U., Hoffmann, T., Andreae, M. O., Meixner, F. X., and Trebs, I.: HONO Emissions from Soil Bacteria as a Major Source of Atmospheric Reactive Nitrogen, Science, 341, 1233–1235, https://doi.org/10.1126/science.1242266, 2013.

Pan, Y. Y., Li, N., Zheng, J. Y., Yin, S. S., Li, C., Yang, J., Zhong, L. J., and Chen, D. H.: Emission inventory and characteristics of anthropogenic air pollutant sources in Guangdong Province Acta Scientiae Circumstantiae, Acta Scientiae Circumstantiae, 35, 2655–2669, 2014.

Pathak, R. K., Wu, W. S., and Wang, T.: Summertime $PM_{2.5}$ ionic species in four major cities of China: nitrate formation in an ammonia-deficient atmosphere, Atmos. Chem. Phys., 9, 1711–1722, https://doi.org/10.5194/acp-9-1711-2009, 2009.

Pathak, R. K., Wang, T., Ho, K. F., and Lee, S. C.: Characteristics of summertime $PM_{2.5}$ organic and elemental carbon in four major Chinese cities: Implications of high acidity for water-soluble organic carbon (WSOC), Atmos. Environ., 45, 318–325, https://doi.org/10.1016/j.atmosenv.2010.10.021, 2011.

Qin, M., Xie, P. H., Su, H., Gu, J. W., Peng, F. M., Li, S. W., Zeng, L. M., Liu, J. G., Liu, W. Q., and Zhang, Y. H.: An observational study of the HONO$-NO_2$ coupling at an urban site in Guangzhou City, South China, Atmos. Environ., 43, 5731–5742, https://doi.org/10.1016/j.atmosenv.2009.08.017, 2009.

Ren, X. R., Harder, H., Martinez, M., Lesher, R. L., Oliger, A., Simpas, J. B., Brune, W. H., Schwab, J. J., Demerjian, K. L., He, Y., Zhou, X. L., and Gao, H. G.: OH and HO_2 chemistry in the urban atmosphere of New York City, Atmos. Environ., 37, 3639–3651, https://doi.org/10.1016/s1352-2310(03)00459-x, 2003.

Sarwar, G., Roselle, S. J., Mathur, R., Appel, W., Dennis, R. L., and Vogel, B.: A comparison of CMAQ HONO predictions with observations from the northeast oxidant and particle study, Atmos. Environ., 42, 5760–5770, https://doi.org/10.1016/j.atmosenv.2007.12.065, 2008.

Stemmler, K., Ndour, M., Elshorbany, Y., Kleffmann, J., D'Anna, B., George, C., Bohn, B., and Ammann, M.: Light induced conversion of nitrogen dioxide into nitrous acid on submicron humic acid aerosol, Atmos. Chem. Phys., 7, 4237–4248, https://doi.org/10.5194/acp-7-4237-2007, 2007.

Stutz, J., Alicke, B., Ackermann, R., Geyer, A., Wang, S. H., White, A. B., Williams, E. J., Spicer, C. W., and Fast, J. D.: Relative humidity dependence of HONO chemistry in urban areas, J. Geophys. Res.-Atmos., 109, D03307, https://doi.org/10.1029/2003jd004135, 2004.

Su, H., Cheng, Y. F., Shao, M., Gao, D. F., Yu, Z. Y., Zeng, L. M., Slanina, J., Zhang, Y. H., and Wiedensohler, A.: Nitrous acid (HONO) and its daytime sources at a rural site during the 2004 PRIDE-PRD experiment in China, J. Geophys. Res.-Atmos., 113, D14312, https://doi.org/10.1029/2007jd009060, 2008.

Su, H., Cheng, Y. F., Oswald, R., Behrendt, T., Trebs, I., Meixner, F. X., Andreae, M. O., Cheng, P., Zhang, Y., and Poschl, U.: Soil Nitrite as a Source of Atmospheric HONO and OH Radicals, Science, 333, 1616–1618, https://doi.org/10.1126/science.1207687, 2011.

Tan, J. H., Duan, J. C., He, K. B., Ma, Y. L., Duan, F. K., Chen, Y., and Fu, J. M.: Chemical characteristics of PM2.5 during a typical haze episode in Guangzhou, J. Environ. Sci., 21, 774–781, https://doi.org/10.1016/s1001-0742(08)62340-2, 2009.

Tham, Y. J., Wang, Z., Li, Q., Yun, H., Wang, W., Wang, X., Xue, L., Lu, K., Ma, N., Bohn, B., Li, X., Kecorius, S., Größ, J., Shao, M., Wiedensohler, A., Zhang, Y., and Wang, T.: Significant concentrations of nitryl chloride sustained in the morning: investigations of the causes and impacts on ozone production in a polluted region of northern China, Atmos. Chem. Phys., 16, 14959–14977, https://doi.org/10.5194/acp-16-14959-2016, 2016.

VandenBoer, T. C., Markovic, M. Z., Sanders, J. E., Ren, X., Pusede, S. E., Browne, E. C., Cohen, R. C., Zhang, L., Thomas, J., Brune, W. H., and Murphy, J. G.: Evidence for a nitrous acid (HONO) reservoir at the ground surface in Bakersfield, CA, during CalNex 2010, J. Geophys. Res.-Atmos., 119, 9093–9106, https://doi.org/10.1002/2013JD020971, 2014

Wang, G., Zhang, R., Gomez, M. E., Yang, L., Zamora, M. L., Hu, M., Lin, Y., Peng, J., Guo, S., Meng, J., Li, J., Cheng, C., Hu, T., Ren, Y., Wang, Y., Gao, J., Cao, J., An, Z., Zhou, W., Li, G., Wang, J., Tian, P., Marrero-Ortiz, W., Secrest, J., Du, Z., Zheng,

J., Shang, D., Zeng, L., Shao, M., Wang, W., Huang, Y., Wang, Y., Zhu, Y., Li, Y., Hu, J., Pan, B., Cai, L., Cheng, Y., Ji, Y., Zhang, F., Rosenfeld, D., Liss, P. S., Duce, R. A., Kolb, C. E., and Molina, M. J.: Persistent sulfate formation from London Fog to Chinese haze, Proc. Natl. Acad. Sci. USA, 113, 13630–13635, https://doi.org/10.1073/pnas.1616540113, 2016.

Wang, J., Zhang, X., Guo, J., Wang, Z., and Zhang, M.: Observation of nitrous acid (HONO) in Beijing, China: Seasonal variation, nocturnal formation and daytime budget, The Sci. Total Environ., 587, 350–359, https://doi.org/10.1016/j.scitotenv.2017.02.159, 2017.

Wang, S. S., Zhou, R., Zhao, H., Wang, Z. R., Chen, L. M., and Zhou, B.: Long-term observation of atmospheric nitrous acid (HONO) and its implication to local NO_2 levels in Shanghai, China, Atmos. Environ., 77, 718–724, https://doi.org/10.1016/j.atmosenv.2013.05.071, 2013.

Wang, T. and Kwok, J. Y. H.: Measurement and analysis of a multiday photochemical smog episode in the Pearl River delta of China, J. Appl. Meteorol., 42, 404–416, https://doi.org/10.1175/1520-0450(2003)042<0404:maaoam>2.0.co;2, 2003.

Wang, T., Lam, K. S., Lee, A. S. Y., Pang, S. W., and Tsui, W. S.: Meteorological and chemical characteristics of the photochemical ozone episodes observed at Cape D'Aguilar in Hong Kong, J. Appl. Meteorol., 37, 1167–1178, https://doi.org/10.1175/1520-0450(1998)037<1167:maccot>2.0.co;2, 1998.

Wang, T., Xue, L., Brimblecombe, P., Lam, Y. F., Li, L., and Zhang, L.: Ozone pollution in China: A review of concentrations, meteorological influences, chemical precursors, and effects, Sci. Total Environ., 575, 1582–1596, https://doi.org/10.1016/j.scitotenv.2016.10.081, 2017.

Wang, X. M., Ding, X., Fu, X. X., He, Q. F., Wang, S. Y., Bernard, F., Zhao, X. Y., and Wu, D.: Aerosol scattering coefficients and major chemical compositions of fine particles observed at a rural site hit the central Pearl River Delta, South China, J. Environ. Sci., 24, 72–77, https://doi.org/10.1016/s1001-0742(11)60730-4, 2012.

Xu, J., Zhang, Y., and Wang, W.: Numerical study on the impacts of heterogeneous reactions on ozone formation in the Beijing urban area, Adv. Atmos. Sci., 23, 605–614, https://doi.org/10.1007/s00376-006-0605-1, 2006.

Xu, Z., Wang, T., Xue, L. K., Louie, P. K. K., Luk, C. W. Y., Gao, J., Wang, S. L., Chai, F. H., and Wang, W. X.: Evaluating the uncertainties of thermal catalytic conversion in measuring atmospheric nitrogen dioxide at four differently polluted sites in China, Atmos. Environ., 76, 221–226, https://doi.org/10.1016/j.atmosenv.2012.09.043, 2013.

Xu, Z., Wang, T., Wu, J. Q., Xue, L. K., Chan, J., Zha, Q. Z., Zhou, S. Z., Louie, P. K. K., and Luk, C. W. Y.: Nitrous acid (HONO) in a polluted subtropical atmosphere: Seasonal variability, direct vehicle emissions and heterogeneous production at ground surface, Atmos. Environ., 106, 100–109, https://doi.org/10.1016/j.atmosenv.2015.01.061, 2015.

Xue, L., Gu, R., Wang, T., Wang, X., Saunders, S., Blake, D., Louie, P. K. K., Luk, C. W. Y., Simpson, I., Xu, Z., Wang, Z., Gao, Y., Lee, S., Mellouki, A., and Wang, W.: Oxidative capacity and radical chemistry in the polluted atmosphere of Hong Kong and Pearl River Delta region: analysis of a severe photochemical smog episode, Atmos. Chem. Phys., 16, 9891–9903, https://doi.org/10.5194/acp-16-9891-2016, 2016.

Xue, L. K., Wang, T., Gao, J., Ding, A. J., Zhou, X. H., Blake, D. R., Wang, X. F., Saunders, S. M., Fan, S. J., Zuo, H. C., Zhang, Q. Z., and Wang, W. X.: Ground-level ozone in four Chinese cities: precursors, regional transport and heterogeneous processes, Atmos. Chem. Phys., 14, 13175–13188, https://doi.org/10.5194/acp-14-13175-2014, 2014.

Ye, C., Gao, H., Zhang, N., and Zhou, X.: Photolysis of Nitric Acid and Nitrate on Natural and Artificial Surfaces, Environ. Sci. Technol., 50, 3530–3536, https://doi.org/10.1021/acs.est.5b05032, 2016a.

Ye, C. X., Zhou, X. L., Pu, D., Stutz, J., Festa, J., Spolaor, M., Tsai, C., Cantrell, C., Mauldin, R. L., Campos, T., Weinheimer, A., Hornbrook, R. S., Apel, E. C., Guenther, A., Kaser, L., Yuan, B., Karl, T., Haggerty, J., Hall, S., Ullmann, K., Smith, J. N., Ortega, J., and Knote, C.: Rapid cycling of reactive nitrogen in the marine boundary layer, Nature, 532, 489–491, https://doi.org/10.1038/nature17195, 2016b.

Ye, C., Zhang, N., Gao, H., and Zhou, X.: Photolysis of Particulate Nitrate as a Source of HONO and NO_x, Environ. Sci. Technol., 51, 6849–6856, https://doi.org/10.1021/acs.est.7b00387, 2017.

Yue, D. L., Zhong, L. J., Zhang, T., Shen, J., Zhou, Y., Zeng, L. M., Dong, H. B., and Ye, S. Q.: Pollution Properties of Water-Soluble Secondary Inorganic Ions in Atmospheric $PM_{2.5}$ in the Pearl River Delta Region, Aerosol Air Qual. Res., 15, 1737–1747, https://doi.org/10.4209/aaqr.2014.12.0333, 2015.

Yun, H., Wang, Z., Zha, Q., Wang, W., Xue, L., Zhang, L., Li, Q., Cui, L., Lee, S., Poon, S. C. N., and Wang, T.: Nitrous acid in a street canyon environment: Sources and contributions to local oxidation capacity, Atmos. Environ., 167, 223–234, https://doi.org/10.1016/j.atmosenv.2017.08.018, 2017.

Yun, H., Wang, W., Wang, T., Xia, M., Yu, C., Wang, Z., Poon, S. C. N., Yue, D., and Zhou, Y.: Nitrate formation from heterogeneous uptake of dinitrogen pentoxide during a severe winter haze in southern China, Atmos. Chem. Phys., 18, 17515–17527, https://doi.org/10.5194/acp-18-17515-2018, 2018.

Zha, Q., Xue, L., Wang, T., Xu, Z., Yeung, C., Louie, P. K. K., and Luk, C. W. Y.: Large conversion rates of NO_2 to HNO_2 observed in air masses from the South China Sea: Evidence of strong production at sea surface?, Geophys. Res. Lett., 41, 7710–7715, https://doi.org/10.1002/2014gl061429, 2014.

Zhang, L., Wang, T., Zhang, Q., Zheng, J., Xu, Z., and Lv, M.: Potential sources of nitrous acid (HONO) and their impacts on ozone: A WRF-Chem study in a polluted subtropical region, J. Geophys. Res.-Atmos., 121, 3645–3662, https://doi.org/10.1002/2015jd024468, 2016.

Zhang, L., Li, Q., Wang, T., Ahmadov, R., Zhang, Q., Li, M., and Lv, M.: Combined impacts of nitrous acid and nitryl chloride on lower-tropospheric ozone: new module development in WRF-Chem and application to China, Atmos. Chem. Phys., 17, 9733–9750, https://doi.org/10.5194/acp-17-9733-2017, 2017.

Zhang, Q., Streets, D. G., Carmichael, G. R., He, K. B., Huo, H., Kannari, A., Klimont, Z., Park, I. S., Reddy, S., Fu, J. S., Chen, D., Duan, L., Lei, Y., Wang, L. T., and Yao, Z. L.: Asian emissions in 2006 for the NASA INTEX-B mission, Atmos. Chem. Phys., 9, 5131–5153, https://doi.org/10.5194/acp-9-5131-2009, 2009.

Zhang, Y. H., Su, H., Zhong, L. J., Cheng, Y. F., Zeng, L. M., Wang, X. S., Xiang, Y. R., Wang, J. L., Gao, D. F., Shao, M., Fan, S. J., and Liu, S. C.: Regional ozone pollution and observation-based approach for analyzing ozone-precursor relationship during the PRIDE-PRD2004 campaign, Atmos. Environ., 42, 6203–6218, https://doi.org/10.1016/j.atmosenv.2008.05.002, 2008.

Zheng, B., Tong, D., Li, M., Liu, F., Hong, C., Geng, G., Li, H., Li, X., Peng, L., Qi, J., Yan, L., Zhang, Y., Zhao, H., Zheng, Y., He, K., and Zhang, Q.: Trends in China's anthropogenic emissions since 2010 as the consequence of clean air actions, Atmos. Chem. Phys., 18, 14095–14111, https://doi.org/10.5194/acp-18-14095-2018, 2018

Zheng, J., Zhong, L., Wang, T., Louie, P. K. K., and Li, Z.: Ground-level ozone in the Pearl River Delta region: Analysis of data from a recently established regional air quality monitoring network, Atmos. Environ., 44, 814–823, https://doi.org/10.1016/j.atmosenv.2009.11.032, 2010.

Zhou, X. L., Gao, H. L., He, Y., Huang, G., Bertman, S. B., Civerolo, K., and Schwab, J.: Nitric acid photolysis on surfaces in low-NO_x environments: Significant atmospheric implications, Geophys. Res. Lett., 30, 2217, https://doi.org/10.1029/2003gl018620, 2003.

Zhou, X. L., Zhang, N., TerAvest, M., Tang, D., Hou, J., Bertman, S., Alaghmand, M., Shepson, P. B., Carroll, M. A., Griffith, S., Dusanter, S., and Stevens, P. S.: Nitric acid photolysis on forest canopy surface as a source for tropospheric nitrous acid, Nat. Geosci., 4, 440–443, https://doi.org/10.1038/ngeo1164, 2011.

Zou, Y., Deng, X. J., Zhu, D., Gong, D. C., Wang, H., Li, F., Tan, H. B., Deng, T., Mai, B. R., Liu, X. T., and Wang, B. G.: Characteristics of 1 year of observational data of VOCs, NO_x and O_3 at a suburban site in Guangzhou, China, Atmos. Chem. Phys., 15, 6625–6636, https://doi.org/10.5194/acp-15-6625-2015, 2015.